MAX-PLANCK-INSTITUT FÜR PLASMAPHYSIK

GARCHING BEI MÜNCHEN

Spatio-temporal Bifurcations in the Driven Nonlinear Drift Wave Equation

ALBERT SALAT, HE KAIFEN*

IPP 6/280 March 1989

* Institute of Low Energy Nuclear Physics, Beijing Normal University
Beijing, China

Die nachstehende Arbeit wurde im Rahmen des Vertrages zwischen dem Max-Planck-Institut für Plasmaphysik und der Europäischen Atomgemeinschaft über die Zusammenarbeit auf dem Gebiete der Plasmaphysik durchgeführt.

Abstract

The nonlinear drift wave equation

$$\Phi_t + a\Phi_{txx} + c\Phi_x + f\Phi\Phi_x + \gamma\Phi = -\epsilon\sin(Kx - \Omega t)$$

with wave-like driving term is analyzed numerically. The location of coexisting attractors, the smooth bifurcations of solutions on them and the catastrophic bifurcations between them are investigated. A global bifurcation of the blue sky catastrophe type is made plausible. Several routes to chaos in the time domain (continuous spectrum) are observed. They may or may not be connected with spatial chaos (soliton-type turbulence). Fourier analysis in space and time reveals the nature of the solutions outside the continua.

1. Introduction

Nonlinear dynamic systems such as maps or ordinary differential equations exhibit a surprising wealth of behaviour, as evidenced by any book on the subject, e.g. /1/. Major topics are the analysis and classification of bifurcations and the routes towards chaotic behaviour. The interplay between theory and numerical experiments has been particularly fruitful for simple paradigm equations such as the Lorentz system or, in the case of external periodic driving, the forced Duffing equation. Space dependence typically changes the equations into partial differential equations. Owing to their complexity their properties as dynamic systems are much less well known.

In the present study we investigate a one-dimensional nonlinear PDE which arises as a simple model equation in the context of driven plasma drift waves /2/. The equation considered is

$$\frac{\partial \Phi}{\partial t} + a\frac{\partial^3 \Phi}{\partial t \partial^2 x} + c\frac{\partial \Phi}{\partial x} + f\Phi\frac{\partial \Phi}{\partial x} + \gamma\Phi + \epsilon \sin(Kx - \Omega t) = 0 \qquad (1)$$

with periodic boundary conditions in x. It has already been studied in a wide range of driving frequencies Ω /2/, /3/. The solution exhibits complicated behaviour which is repeated to some extent in cell-like domains of decreasing size for $\Omega \to 0$. Hysteresis and various bifurcations have been observed but have been studied in a rather preliminary way. The aim here is to do a systematic study of the attractors present and of the smooth and catastrophic bifurcations, respectively, on and between coexisting attractors. We try to separate local bifurcations from global ones, caused by collision with unstable manifolds. New types of solution and new routes to chaotic time behaviour in comparison with the previous work on equ. (1) are identified. Chaos in time is found to be not always accompanied by chaos in space. We concentrate on the cell in the region $0.44 \leq \Omega \leq 0.65$, which exhibits a rich and typical variety of phenomena.

In Section 2 we present the solution $\Phi(x,t)$ and the energy $E(t)$, as a classification scheme, for a few selected values of Ω as functions of the driving amplitude ϵ. Section 3 puts these pieces together into a state diagram $\epsilon(\Omega)$. In Section 4 we try to interpret the bifurcations observed. Some of them may be understood in terms of how equ. (1) is related to the driven Duffing equation. Section 5 contains a summary of the results obtained.

2. Spatio-temporal properties

Equation (1) contains seven free parameters. We study the dependence of the solution $\Phi(x,t)$ on the amplitude ϵ and frequency Ω of the driving term $\epsilon \sin(Kx - \Omega t)$. The other coefficients are kept fixed throughout. The values $a = -0.28711$, $c = 1.0$, $f = -6.0$, $\gamma = 0.1$ and $K = 1$ are chosen as in previous work /2/, /3/. In this section, we restrict the discussion to a few typical values of Ω and study the continuous dependence on the amplitude ϵ.

Equation (1) is solved numerically with periodic boundary conditions, with the spectral ansatz

$$\Phi(x,t) = \sum_{k=0}^{N-1} \Phi_k(t) \exp(\, ikx \,) \qquad \text{at} \quad x = x_j = \frac{2\pi j}{N}, \quad j = 0, \ldots N-1. \tag{2}$$

The nonlinear term is evaluated in coordinate space with N grid points by using fast Fourier transformation with dealiasing. For nonchaotic solutions $N = 128$ is usually sufficient. Time integration of the ordinary differential equations for $\mathrm{d}\Phi_k/\mathrm{d}t$ is performed with a standard predictor-corrector scheme with time step $\Delta t = 10^{-2}$ in most runs.

Depending on the situation, initial transients die away at appreciably different rates, ranging from smooth decay to sudden explosive transitions. Thus, (quasi-)stationary situations are obtained after times t_0 ranging from 10 to 10^4. Transients will not be shown here.

A very useful means of discriminating between different classes of solution is the time dependence of the energy $E(t)$, which is defined as

$$E(t) = \frac{1}{2\pi} \int_0^{2\pi} \frac{1}{2} \left[\Phi^2(x,t) - a \left(\frac{\partial \Phi(x,t)}{\partial} x \right)^2 \right] \mathrm{d}x \quad . \tag{3}$$

In the absence of driving and damping $E(t)$ is a constant of the motion.

In the following $E(t)$ and the solution $\Phi(x,t)$ will be discussed at $\Omega = 0.48$, 0.525, 0.59, 0.625 and 0.65. The values are selected in such a way that new features occur at each frequency.

$\underline{\Omega = 0.48:}$

At small driving amplitudes ϵ the energy $E(t)$ becomes constant asymptotically (see Fig. 1a) just as in the case $\epsilon = \gamma = 0$. The solution $\Phi(x,t)$ is a plane wave moving with the phase velocity $u = \Omega/K$ of the driving term (see Fig. 1b). The Fourier transform $\widehat{\Phi}(\omega)$ of Φ with respect to t at a fixed position is composed of integer multiples of the driving frequency Ω.

With increasing ϵ, this situation continues until around $\epsilon = 0.067$, where $E(t)$ becomes slightly periodic with frequency $\omega_E = 0.683$ (see Fig. 2a). (The time interval in this and all analogous figures is $\Delta t = 800$.) To the eye the solution $\Phi(x,t)$ still looks qualitatively unchanged (see Fig. 2b). (In the figures of $\Phi(x,t)$ the time interval is much less, $\Delta t = 36$. The zero of the ordinate is such that the space average $< \Phi >$ is zero, in conformity with $d < \Phi > /dt = -\gamma < \Phi >$ and $\gamma t >> 1$.)

Just above $\epsilon = 0.067$ the solution is abruptly changed in type into a state with higher energy and more vigorous motion; see, for example, Figs. 3a, 3b. If such a higher-branch solution $\Phi(x,t)$ is used as initial condition, but with ϵ decreased, the higher-branch solution is found to coexist in a narrow ϵ interval with the lower branch. The situation, with the concurrent hysteresis loop, say between ϵ_l and ϵ_h, is shown schematically in the insert of Fig. 8. Figures 3a, 3b contain the higher-branch solution at $\epsilon = 0.067$, coexisting with that of Figs. 2a, 2b. $E(t)$ is a quasiperiodic function based on the two incommensurate frequencies $\omega_E = 0.679$ and $\omega'_E = 0.023$ and their multiples, as is evident from the spectrum

$\widehat{E}(\omega)$ shown in Fig. 3c. The solution $\Phi(x,t)$ in Fig. 3b retains the basic wave-like structure of the lower branch, with the periodic sequence of high and low maxima. Superimposed on it, however, is a strong wave-like motion in the opposite direction. The spectrum $\widehat{\Phi}(\omega)$ is based on the same fundamental frequencies as $\widehat{E}(\omega)$, in addition to the driving frequency Ω. This property is observed in all cases considered. It is therefore more useful to concentrate on $\widehat{E}(\omega)$, which is free of the trivial $n\Omega$ lines, $n = 1, 2, \ldots$.

With ϵ decreased slightly more, the higher branch has a periodic $E(t)$ with large amplitude (see Figs. 4a, 4b). Obviously, the smooth transition $E(t)$ = constant $\rightarrow$ weakly periodic $\rightarrow$ more strongly periodic $\rightarrow$ weakly quasiperiodic, etc. is interrupted by a fold (see insert in Fig. 8), so that part of this transition is obscured from view by instability.

When the driving amplitude is further increased the quasiperiodic character of $E(t)$ becomes more pronounced. At the same time $\Phi(x,t)$ becomes "rougher": see Figs. 5a, 5b for $\epsilon = 0.07$. While ω_E stays constant, ω'_E decreases and the number of harmonics in the spectrum grows. Between $\epsilon = 0.071$ and 0.072 the spectrum practically becomes dense, with just the frequency ω_E standing out from the continuum. At the same time $\Phi(x,t)$ develops localized humps of the soliton type. Figures 6a - 6c show the situation at the slightly higher value $\epsilon = 0.08$. $E(t)$ is an intermittent function, the basic oscillations being interrupted by stochastic bursts. Soliton-like features persist for some time until they merge or decay.

Obviously, there is a transition taking place in the character of the solution: local effects with characteristic length $\ll$ periodicity interval become dominant. We call this regime "chaotic" since the "solitons" seem to occur more or less at random positions. Details of the chaotic regime will not be discussed here.

At still higher driving amplitude the number of "solitons" grows until they dominate the whole interval; see Fig. 7b for $\epsilon = 0.12$. The intermittent behaviour of $E(t)$ has given way to a smoother stochastic function (see Fig. 7a). The number of grid points should be increased in cases with pronounced soliton behaviour. We used $N = 256$ and $N = 512$ in

test runs. Apart from better resolution the phenomena are unchanged.

The properties of the solution for $\Omega = 0.48$ so far discussed are collected in the bifurcation diagram in Fig. 8, which shows the energy E versus the driving amplitude ϵ. For nonsteady $E(t)$ the minimum and maximum values during some reasonably large time interval are given, connected by vertical lines. The symbols mean: ($\circ$) periodic, (Δ) quasiperiodic $E(t)$; ($\times$) stands for chaotic $\Phi(x,t)$ (i.e. with "solitons"), here in conjunction with a continuous spectrum. The chaotic regime is seen to join smoothly to the quasiperiodic one. Both the average energy and its variation $\Delta E = E_{max} - E_{min}$ grow steeply with increasing ϵ in these regimes. The insert shows schematically the narrow hysteresis discussed above. Each fold originates from a saddle-node coalescence of stable and unstable cycles.

$\underline{\Omega = 0.525:}$

Figure 9 shows the bifurcation diagram $E(\epsilon)$. While the upper part of the figure is qualitatively unchanged, an additional big hysteresis loop has developed at intermediate values of ϵ. The arrows indicate the position of the jumps from one branch to the other which occur at $\epsilon = \epsilon_L = 0.0510$ and $\epsilon = \epsilon_H = 0.0643$. In the hysteresis regime two different solutions with constant $E(t)$ coexist. Figures 10a and 10b show the low-branch solution (L) and the high-branch solution (H), respectively, for $\epsilon = 0.06$. Both are plane waves with $u = \Omega/K$, and the H-solution resembles $\Phi(x,t)$ from Fig. 1b.

All bifurcation diagrams were obtained by the step-by-step method: the solution $\Phi(x,t)$ at some arbitrary time t in the (quasi-)steady-state regime is used as initial condition for a run whose value ϵ is increased or decreased by a small amount $\Delta\epsilon$. Ideally, $\Delta\epsilon$ should be infinitesimally small. In practice, a compromise between accuracy and expenditure of time is necessary. With respect to the chaotic branch this occasionally causes problems (see below).

$\Omega = 0.59$:

At higher values of Ω the hysteresis between the L- and H-branches becomes more extended. In particular, the upper end of the hysteresis, ϵ_H, grows. As a consequence, for $\Omega \gtrsim 0.55$ the L-branch jumps into the periodic, the quasiperiodic or even the chaotic part of the H-branch.

A new phenomenon is evident in Fig. 11, the bifurcation diagram for $\Omega = 0.59$: the low branch develops an extended section with periodic $E(t)$(see Fig. 12a). Analysis shows that the transitions to and from periodicity at the two critical values $\epsilon = \epsilon_o = 0.0717$ and 0.128 are Hopf bifurcations: the periodic part of $E(t)$ grows as $|\epsilon - \epsilon_o|^{\frac{1}{2}}$ in the vicinity of the bifurcation points, while the frequency ω_E stays approximately constant. $\Phi(x,t)$ resembles the previous L-branch type. What used to be plane waves, however, is now twisted back and forth during wave propagation. This $\Phi(x,t)$ (Fig. 12b) is quite different from the periodic cases in the higher branch, as comparison with Fig. 4b shows.

While the L-branch develops a periodic section, the H-branch develops a gap (see Fig. 11). The latter sets in at the end of the quasiperiodic part or right after the beginning of the chaotic part in which it grows. The values of $E(t)$ after the chaotic part re-emerges exceed the scope of the figure. The underlined crosses in the upper right corner are therefore meant to indicate the extent of this branch with respect to ϵ only. The main section of the high branch can now no longer be reached by the step-by-step method. Experience shows that it is attainable by starting with a simple sinusoidal function $\Phi(x, t = 0)$ with a sufficiently negative constant added.

The preliminary end of the H-branch at $\epsilon = 0.109$ offers a good opportunity to study $\Phi(x,t)$ in the intermittent state, already observed at lower Ω also. Figure 13a shows a pronounced case. The two horizontal bars indicate a quiet phase and a strong peak in $E(t)$. Figures 13b, 13c show $\Phi(x,t)$ during these two intervals. In the quiet phase, Fig. 13b, the solution is still basically a plane wave, while during the peak, Fig. 13c, backward

moving local humps and crests are superposed on the waves.

Finally, the narrow hysteresis observed at $\Omega = 0.48$ and in the H-branch at $\Omega = 0.525$ has levelled out here at $\Omega = 0.59$. The transition from $E = \text{const}$ via Hopf bifurcation to periodic E and further via secondary Hopf to quasiperiodic E has become a continuous process.

$\Omega = 0.625$:

The bifurcation diagram is given in Fig. 14. The low branch offers a new feature again: the periodic section is interrupted by a section with period doubling (marked by pluses (+)) between $\epsilon = \epsilon_+ = 0.167$ and 0.179. The function $E(t)$ and its spectrum at $\epsilon = 0.167$ in this regime are given in Figs. 15a and 15c. Apart from the dominant frequency $\omega_E = 0.338$, which is close to the value in the periodic section, its subharmonic $\omega_E/2$ is evident. The period doubling refers to ω_E only. There are no components with $\Omega/2$ in the spectrum $\widehat{\Phi}(\omega)$. The solution $\Phi(x,t)$ in Fig. 15b, although more vigorous than in the periodic situation, is still of the twisted-wave type.

$\Omega = 0.65$:

This is the highest value of the driving frequency Ω considered here. A host of new phenomena arise. To the bifurcation diagram, Fig. 16, a schematic one, Fig. 17, is added in order to bring out the details.

A fold develops in what used to be the low branch, dividing it up into two sub-branches, (I) and (II). The periodic part of the low branch, branch (II) in Fig. 17, extends up to $\epsilon = \epsilon_\infty = 0.1926$, where it jumps (slightly) down to the lower pleat. Branch (I) is marked with black squares in Fig. 16. It begins at $\epsilon = 0.1774$ with a period-doubled state with

respect to $\omega_E = 0.403$. This state changes smoothly into a situation with ω_E, $\omega_E/2$ and an incommensurate frequency ω'_E. Figures 18a and 18c show $E(t)$ and $\widehat{E}(\omega)$ at $\epsilon = 0.182$ in this regime, with $\omega_E = 0.399$ and $\omega'_E = 0.054$. Just as in the quasiperiodic part of the H-branch an increase of ϵ decreases ω'_E and increases the number of harmonics of ω'_E in $\widehat{E}(\omega)$ until the spectrum is practically continuous except for broad peaks around ω_E and $\omega_E/2$. This occurs at $\epsilon = \epsilon'_\infty \approx 0.188$ (see Figs. 19a, 19c). Around $\epsilon = 0.185$ there is also a small region with mode locking of ω'_E with $\omega_E/8$. Further increase of ϵ across ϵ'_∞ brings the system back to a period -doubled state. This is followed by a whole period-doubling sequence, with $\omega_E/4$, $\omega_E/8$, $\omega_E/16$ etc. occurrin in ever faster succession and crowding the spectrum until $\widehat{E}(\omega)$ again becomes a continuum at $\epsilon_\infty = 0.1926$. It is probably no coincidence that branch (II) ends right at this value of ϵ. The continuum state extends up to $\epsilon = 0.2005$, where it jumps up into the chaotic state. Figures 20a, 20c at $\epsilon = 0.200$ show $E(t)$ and $\widehat{E}(\omega)$ in the continuum region, while Figs. 21a, 21b have $\epsilon = 0.201$ and show the strong soliton chaos after the jump.

It remains to discuss the space dependence of the solution in the L-branches. In order to appreciate the result, it is useful to remember the behaviour in the H-branch (or at $\Omega = 0.48$, which is equivalent to it in this respect). In this branch, if we disregard the plane wave solutions, $\Phi(x,t)$ has strong backward moving components: see, for example, Figs. 3b, 4b. With increasing ϵ, the spectrum $\widehat{E}(\omega)$ becomes denser until it becomes continuous. At the same time the backward moving components become stronger until everything piles up to chaotic solitons with a continuous spectrum in k also. Thus, the behaviour in *space* and the behaviour in *time* are closely *linked* in the H-branch.

In the L-branch non-plane-wave solutions encountered so far are of the smooth twisted-wave type, see, for example, Fig. 15. At $\Omega = 0.65$ the L-branch (II) with increasing ϵ acquires some backward motion also: see Fig. 18b at $\epsilon = 0.182$. This continues into the beginning of branch (I), but with further increasing ϵ, the tendency is back to the twisted-wave type. Nevertheless, as discussed above, the spectrum $\widehat{E}(\omega)$ becomes denser and

denser and reaches a continuum at ϵ'_∞ and again at ϵ_∞. As a consequence, a chaotic time dependence with a continuous spectrum $\widehat{E}(\omega)$ coexists with a smooth space dependence. This situation is shown in Figs. 19a-c and 20a-c at $\epsilon = 0.188$ and 0.200, respectively. They prove that the behaviour in space and that in time are *not* closely linked here.

3. State diagram

In the last section the properties of the solution of equ. (1) and the resulting bifurcations were studied at a few selected values of the driving frequency Ω. Here we sum up this study and fashion it into the state diagrams in Figs. 22 and 23 in the (ϵ, Ω) plane.

Different types of solution are marked by different symbols according to the properties of $E(t)$. Dots ($\bullet$), circles ($\circ$) and pluses ($+$) denote $E(t)$ = const, periodic and period-doubled, respectively, while squares, circles with plus ($\oplus$) and crosses ($\times$) indicate period-quadrupled (or higher), quasiperiodic and chaotic energies, respectively. Coexistence of two different branches is marked by two symbols beside each other.

The end of a branch, i.e. a catastrophic bifurcation, is marked by a solid curve. Dotted curves correspond to smooth transitions from one type of solution to another, i.e. to continuous bifurcations. The catastrophic end of chaotic sections is not marked by a solid curve but by a dashed one in order to indicate a less reliably determined course. (As mentioned in the previous section, precisely locating the jump out of strongly fluctuating soliton-type solutions requires a great deal of effort. It may not even be well defined but could be a function of the moment at which ϵ is infinitesimally modified.)

Figure 22 shows the situation in the region Ω = 0.44 - 0.65, which has already been investigated in a very preliminary way /2/. Arrows at the bottom of the figure indicate those values of Ω which were extensively discussed in Section 2. The main features are the pointed "horn" ending in a cusp at $\Omega \approx 0.50$, the rounded-off horn ending at $\Omega \approx 0.458$, and the dotted Hopf bifurcation curve ϵ_o.

The pointed horn consists of the upper boundary ϵ_H of the L-branch and the lower boundary ϵ_L of the H-branch. Of course, there is an unstable fold connecting the two branches.

The narrow hysteresis between ϵ_l and ϵ_h forms the bottom of the rounded horn. ϵ_h

turns upward and to the right at $\Omega \approx 0.458$, thus creating the horn in which $E(t)$ is chaotic except in the lower boundary region. To the left of $\Omega = 0.458$ the $E = \text{const}$ branch exists without interruption for all ϵ (inside the bounds of Fig. 22). The "envelope" of the horn, which includes periodic, quasiperiodic and chaotic $E(t)$, continues to the left until it vanishes at $\Omega \approx 0.41$.

The rounded horn meets ϵ_H at $\Omega \approx 0.55$. At this point the narrow hysteresis vanishes in another cusp and the bottom of the horn continues as a smooth bifurcation inside the H-branch. Where it collides with the Hopf curve ϵ_o at $\Omega \approx 0.58$ a new pair of catastrophic bifurcations is created, which opens up a gap in the H-branch. At low ϵ the gap is bounded by the end of the quasiperiodic region ($\oplus$), solid curve, and at higher ϵ by the end of the chaotic region ($\times$), dashed. Since the dashed curve almost parallels the Hopf curve ϵ_o it is tempting to speculate that the H-branch attractor is destroyed by collision with the aforementioned unstable manifold which connects the L- and H-branches and which presumably is also periodic in this region. The location of the lower end of the gap supports this view: quasiperiodic solutions are much less extended in phase space than chaotic ones, by definition as it were. Hence, they are less likely to collide with the neighbouring unstable manifold. The bifurcation therefore seems to be of a global type, called "blue sky catastrophe" in /4/ and /5/, and is analogous to a boundary crisis of Grebogi, Ott and York /6/. The collision may involve a homoclinic orbit, which is presumably present in phase space (see next section).

In the upper right corner of Fig. 22 additional features exist, which are shown enlarged in Fig. 23. ϵ_H and the almost parallel reverse Hopf bifurcation ϵ_o are still continuations from Fig. 22. The lower end of the chaotic branch (dashed) veers away from ϵ_H, ϵ_o and moves obliquely across the figure. New, however, are the period-doubling region (+), and its inclusions, the period-quadrupling (and higher) region (square) and the quasiperiodic region ($\oplus$). The two solid curves to the right mark the lower end of the L-branch (I) and the upper end of the L-branch (II).

It is evident that at the two values of Ω, $\Omega_1 = 0.6287$ and $\Omega_2 = 0.6415$, which are marked on the axis, an abrupt change of the underlying attractors takes place: at $\Omega = \Omega_1$ the period -quadrupling region ends while the period-doubling region grows discontinuously. At $\Omega = \Omega_2$ the fold in the L-branch begins, which creates the branches (I) and (II). At the same time the extent of the L-branch shrinks until its boundary ϵ_H seems to coincide with the boundary of the (chaotic) H-region. The dashed curve should therefore be understood as coinciding with a solid curve ϵ_H. The previously existing finite overlap between L and H is destroyed, and with it the sequence period quadrupled $\rightarrow$ doubled $\rightarrow$ periodic $\rightarrow$ const, which takes place at lower values of Ω.

The nature of these events at Ω_1 and Ω_2 which are reminiscent of interior crises, is not yet known. Collisions with homoclinic orbits may be involved.

4. Discussion

In order to understand at least some of the bifurcations observed, it is useful to consider first those cases in which the solution $\Phi(x,t)$ depends on $t' = t - K\,x\,/\,\Omega$ only, i.e. solutions whose phase velocity coincides with that of the driving term. With the spatial periodicity assumption for $\Phi(x,t)$, equ. (3) in this case immediately yields $E(t) = \text{const}$. This fits the numerical observations that $E = \text{const}$ cases, (•), always have plane-wave -type $\Phi(x,t)$; see Figs. 1a, 1b and Figs. 10a, 10b.

Equation (1) transforms to

$$aK^2\,\dddot{\Phi} + \Omega(\Omega - cK)\,\dot{\Phi} + \gamma\Omega^2\,\Phi - fK\Omega\,\Phi\dot{\Phi} = \epsilon\Omega^2\,\sin(\Omega t') \quad , \tag{4}$$

where the dot means $\partial/\partial t'$. If for the moment the damping is neglected by putting $\gamma = 0$, equ. (4) can be integrated once. Putting a damping term, say $\mu\,\dot{\Phi}$, back on yields

$$\ddot{\Phi} + \mu\,\dot{\Phi} + r\,\Phi + s\,\Phi^2 = \delta\,\cos(\Omega t') \quad , \tag{5}$$

with $r = \Omega(\Omega - cK)/(aK^2)$, $s = -fK\Omega/(2aK^2)$, $\delta = -\epsilon\Omega/(aK^2)$ and μ proportional to γ. This is a Duffing-type equation with potential $V(\Phi) = r\Phi^2/2 + s\Phi^3/3$, with $r > 0$ for $0 < \Omega < 1$ and $s < 0$ for our choice of parameters. The undriven, undamped equation is derived from the Hamiltonian $H(\Phi,\dot{\Phi}) = r\Phi^2/2 + s\Phi^3/3 + \dot{\Phi}^2/2$ and contains a saddle and a homoclinic orbit.

Duffing equations with various (single- and double-humped) potentials $V(\Phi)$ are one of the paradigms of nonlinear dynamics and are treated in most books on the subject: see, for example, /1/ and /7/. Duffing equations offer a rich variety of phenomena. Nonlinearity skews the resonance curves and causes hysteresis. Period doubling and transition to chaos are observed /8/. Subharmonic and ultrasubharmonic resonances lead to a superstructure

of cell- or horn-like regions in amplitude-frequency space /9/. Homoclinic tangency with fractal basin boundaries and crises are observed /5/, /10/ and /11/.

Classical methods for ODEs, such as harmonic balance, e.g. in /12/, can be used to derive approximate analytical results on stability and bifurcations. In our diagrams the only bifurcations between E = const solutions take place in the low-Ω part of the ϵ_H - ϵ_L hysteresis but we shall not analyze it here. It is useful, however, to have a simple model for locating the most prominent resonances to be expected. The "oscillator" of the left-hand side of equ. (4) should show a particularly vigorous reaction to the periodic driving term whenever the driving frequency equals a harmonic of the oscillator's eigenfrequency Ω_0. Amplitude-dependent, exact eigenfrequencies of solitary-wave-type solutions in the case of zero damping are well known /2/ and can be used to discuss the resonance conditions, /13/. Here, however, it suffices to consider the linearized oscillator. With the ansatz $\Phi(t') \sim \exp(i\Omega_0 t')$ and the resonance condition $\Omega = n\Omega_0$, equ. (4) with $\gamma = \epsilon = 0$ yields

$$\Omega = \Omega_n = K \frac{c}{1 - an^2K^2}, \quad n = 1, 2, \ldots . \tag{6}$$

With the parameters chosen above one obtains $\Omega_1 = 0.777$, $\Omega_2 = 0.465$ and $\Omega_3 = 0.279$ (not to be confused with Ω_n in Sec. 3). Thus, in the present range $\Omega = 0.44$ - 0.65 the $n = 2$ resonance should play a rôle. This is indeed observed. For $\Omega = 0.525$, for example, $\omega = 2\Omega$ is the strongest line in the spectrum $\widehat{\Phi}(\omega)$ in the L-branch in the interval $\epsilon_L < \epsilon < \epsilon_H$. In the H-branch it is the second strongest, after the fundamental $\omega = \Omega$. The values Ω_n, $n = 2, 3...$ up to 18 agree well with the positions of "cells" observed in the extended overview for equ. (1) in /2/.

Investigation of equ. (4) would of course also reveal period-doubling phenomena, etc. Such solutions, however, are excluded from our numerical results by the built-in restriction to fixed periodicity length 2π, because for a plane-wave solution period doubling is connected with prohibited periodicity length doubling.

Thus, equ. (1) is not allowed to "do" very much with plane -wave solutions. The previous sections show how it uses its freedom as PDE for solutions other than plane waves. As mentioned in Section 2, the possibility to period-double in $T = 2\pi/\Omega$, with the longest scale length now being fixed and the phase velocity being halved, is not realized. What actually happens is revealed by Fourier decomposition into waves $\widehat{\Phi}_k(\omega)$ according to $\Phi(x,t) = \sum_k \sum_\omega \widehat{\Phi}_k(\omega)) \exp\big(i(kx - \omega t)\big)$. Figures 24 and 25 present two typical cases. The first is an example of the twisted-wave-type solution encountered in the L-branch (see Fig. 12b), while the second is typical of the H- (and h-) branch with its counterpropagating components (see Fig. 4b). Both figures show $\widehat{\Phi}_k(\omega)$ for $\omega > 0$ (solid) and $\omega < 0$ (dashed) for $k = 1$.

The highest line in Fig. 24 is at the driving frequency $\Omega = 0.59$. All other lines present are at positions $\omega = \omega_{1,m} = \Omega + m\omega_E$, $m = \pm 1, \pm 2, \ldots$, where $\omega_E = 0.330$ is the Hopf frequency of the periodic $E(t)$. With increasing $|m|$ the amplitudes quickly decrease, so that in particular the negative frequencies, $\omega_{1,-2}$, $\omega_{1,-3}$ etc., are negligibly small. Essentially all phase velocities $u_{1,m} = \omega_{1,m}/k = (\Omega + m\omega_E)/K$ are positive and are centred around $u = \Omega/K$ of the driving term $\sim \sin(Kx - \Omega t)$. For $k = 2$ the spectrum is of the same type, with lines at $\omega = \omega_{2,m} = 2\Omega + m\omega_E$, $m = 0, \pm 1, \pm 2, \ldots$. Again the phase velocities $u_{2,m} = \omega_{2,m}/k = (\Omega + m\omega_E/2)/K$ are centred around Ω/K, and analogously for higher k. This gives the twisted-wave type of Fig. 12b.

Somewhat unexpectedly, it turns out that the "counterpropagating" case (Fig. 4b) is not basically different (see Fig. 25). Again, at $k = 1$ the highest component is $\omega = \Omega$ $(= 0.48)$ and all other lines are at $\omega_{1,m}$. The only difference is that the decay with $|m|$ is slower and ω_E is larger. As a consequence, $\omega_{1,-1} = \Omega - \omega_E$ is already negative and only a factor of 5.5 smaller than the fundamental. For $k \geq 2$ the situation is similar. This explains the backward motion observed.

Analogously, for period-doubled and quasiperiodic energy $E(t)$ the spectrum $\widehat{\Phi}_k(\omega)$ consists of lines $\omega_{k,m} = k\Omega + m\omega_E/2$ and $\omega_{k,m,l} = k\Omega + m\omega_E + l\omega'_E$, respectively, etc. For

chaotic $E(t)$ the line $\omega = k\Omega$ stands out from an otherwise continuous spectrum $\widehat{\Phi}_k(\omega)$. In these cases spatially chaotic and spatially regular behaviour are associated with lack of decay and rapid decay, respectively, of the mode amplitudes with respect to k.

It should be possible to derive analytic results on local bifurcations by generalizing, for example, the harmonic balance method from pure oscillations to wave-like modes. For an insight into global bifurcations, however, it is indispensable to have a knowledge of the complete phase portrait. In view of its infinite dimensions some kind of diagnostic reduction would obviously be necessary.

5. Conclusions

The *partial* differential equation (1) with periodic boundary conditions was studied numerically in a finite region of amplitude ϵ and frequency Ω of a driving wave $\epsilon \sin(Kx - \Omega t)$. In contrast to previous preliminary investigations /2/, /3/, the location of attractors, the properties of the solutions on them, and the bifurcations both on the attractors (smooth bifurcations) and between coexisting attractors (catastrophic bifurcations) were systematically studied.

With increasing amplitude and frequency a variety of phenomena unfolds. These are collected in the state diagrams Figs. 22 and 23, which show the regions of different behaviour of the energy $E(t)$. In addition to the known types of constant, periodic, quasiperiodic or chaotic energy $E(t)$, period-doubled, period-quadrupled, etc. types with respect to a Hopf frequency ω_E were discovered. Continua in the frequency ω were found to be approached either by a period-doubling sequence in ω_E or by decrease of a secondary Hopf frequency ω'_E.

The bifurcation diagrams $E(\epsilon)$ are less packed with information and therefore better suited to describe, for example, the coexistence of different branches; see Figs. 8, 9, 11, 14, 16 and 17 at selected values of Ω.

The solutions $\Phi(x,t)$ themselves are presented graphically for most of the typical cases mentioned above. Away from the frequency continua all solutions are of the form

$$\Phi(x,t) = \sum_{n\neq 0}\sum_{m,l}\sum_{r\neq 0} \Phi_{n,m,l,r} \exp\{ in[Kx - (\Omega + \frac{m}{nr}\omega_E + \frac{l}{n}\omega'_E)\, t\,]\} \quad , \qquad (7)$$

with $\Phi_{n,m,l,r}$ rapidly declining for large $|n|$, $|m|$, $|l|$, $|r|$. They consist of waves whose phase velocity is the same ($m = l = 0$) as that of the driving term or is staggered symmetrically around it. ($\Phi_{n,m,l,r} = \Phi_{n,m}\delta_{l,0}\delta_{r,1}$ for periodic $E(t)$, $\Phi_{n,m,l,r} = \Phi_{n,m}\delta_{l,0}\delta_{r,2}$ for period

-doubled, etc., and $\Phi_{n,m} = \Phi_n \delta_{m,0}$ for constant E.)

In the frequency continua the space dependence may be regular, e.g. in Fig. 20b, or quite chaotic, as in Fig. 21b, so that "chaos" in time may or may not coexist with "chaos" in space. This qualitative result agrees with the finding of Bishop et al. /14/, whose work on the driven sine-Gordon equation is to some extent related to ours.

"Chaos" in space is often connected with the presence of stationary soliton-like humps (see Fig. 7b). Their dynamics and relation to solitary solutions of the undriven, undamped equation (1) /15/ have not yet been analyzed.

The existence of a global bifurcation, in the form of a blue sky catastrophe /4/, and of interior crises was made plausible. For PDEs, however, it is difficult to give a clear analysis owing to the lack of stringent diagnostic tools in infinite-dimensional phase space. The observation of the energy $E(t)$, defined in equ. (3), is to some extent a global substitute for the Poincaré section method of ODEs for infinite-dimensional PDEs. The analogue between the two methods is that a solution $\Phi(x,t)$ which depends periodically on $x - ut$ is mapped onto a point $E(t) = \text{const}$, here, just as a periodic $\Phi(t)$ is mapped onto a point on a Poincaré section. The *one-dimensional* parameter E, however, cannot compete with the information in a *two-dimensional* Poincaré plane.

References

/ 1/ J. Guckenheimer and P. Holmes, Nonlinear Oscillations, Dynamical Systems, and Bifurcation of Vector Fields, Springer, Berlin, 1986.

/ 2/ He Kaifen and A. Salat, Plasma Phys. and Contr. Fus. 31, 123 (1989).

/ 3/ He Kaifen and A. Salat, Phys. Lett. A 132, 175 (1988).

/ 4/ R. Abraham and H. Stewart, Physica 21*D*, 394 (1986).

/ 5/ J. Thompson, S. Bishop and L. Leung, Phys. Lett. A 121, 116 (1987).

/ 6/ C. Grebogi, E. Ott and J. Yorke, Physica 7*D*, 181 (1983).

/ 7/ J. Thompson and H. Stewart, Nonlinear Dynamics and Chaos, J. Wiley, Chichester, 1986.

/ 8/ B. Huberman and J. Crutchfield, Phys. Rev. Lett. 43, 1743 (1979).

/ 9/ U. Parlitz and W. Lauterborn, Phys. Lett. A 107, 351 (1985).

/10/ F. Moon and G. Li, Phys. Rev. Lett. 55, 1439 (1985).

/11/ R. Raety, J. von Boehm and H. Isomaeki, Phys. Rev. A 34, 4310 (1986).

/12/ C. Hayashi, Nonlinear Oscillation in Physical Systems, McGraw-Hill, New York, 1964.

/13/ He Kaifen and A. Salat, to be published.

/14/ A. Bishop, K. Fesser, P. Lomdahl *et al.* Physica 7*D*, 259 (1983).

/15/ J.D. Meiss and W. Horton, Phys. Fluids 25, 1838 (1982).

Figure captions

Figs. 1a-7a: Energy *vs.* time at $\Omega = 0.48$ at indicated values of ϵ. The time interval is $\Delta t = 800$; Figs. 2a, 3a show coexisting solutions in the l- and h-branches.

Figs. 1b-7b: Solutions $\Phi(x,t)$ at parameter values corresponding to Figs. 1a - 7a. The time interval is $\Delta t = 36$.

Fig. 3c: Energy spectrum $\widehat{E}(\omega)$ at parameter values of Figs. 3a, 3b. Quasiperiodic case based on harmonics of $\omega_E = 0.679$ and $\omega'_E = 0.023$.

Fig. 6c: Energy spectrum $\widehat{E}(\omega)$ at parameter values of Figs. 6a, 6b. Continuous case with "solitons".

Fig. 8: Bifurcation diagram of energy E *vs.* driving amplitude ϵ at $\Omega = 0.48$. Vertical bars indicate maximal extent of nonconstant $E(t)$. Insert shows narrow hysteresis. Symbols $\circ$, Δ and $\times$ denote periodic, quasiperiodic and chaotic $E(t)$, resp.

Fig. 9: Bifurcation diagram at $\Omega = 0.525$. Hysteresis between L- and H-branches is indicated by arrows.

Fig. 10a: Solution $\Phi(x,t)$ in L-branch. $\epsilon = 0.06$; $\Omega = 0.525$.

Fig. 10b: Solution $\Phi(x,t)$ in H-branch at the same parameter values.

Fig. 11: Bifurcation diagram at $\Omega = 0.59$. Underlined crosses in the upper right part indicate chaotic $E(t)$ whose extent exceeds the scope of the figure.

Figs. 12a-c: a) energy $E(t)$, b) solution $\Phi(x,t)$ and c) energy spectrum $\widehat{E}(\omega)$ in periodic case of L-branch. $\epsilon = 0.09$; $\Omega = 0.59$.

Figs. 13a-c: a) energy $E(t)$ in chaotic case. Solution $\Phi(x,t)$ in time intervals indicated by bars: b) quiet phase, and c) peak. ϵ =0.109, Ω =0.59.

Fig. 14: Bifurcation diagram at $\Omega = 0.625$. Symbols + denote period-doubled $E(t)$.

Figs. 15a-c: a) energy $E(t)$, b) solution $\Phi(x,t)$ and c) energy spectrum $\widehat{E}(\omega)$ in period-doubled case of L-branch. $\epsilon = 0.167$; $\Omega = 0.625$.

Fig. 16: Bifurcation diagram at $\Omega = 0.65$. Black squares denote sub-branch (I).

Fig. 17: Details of energy $E(t)$ in sub-branch (I). Locations of sub-branch (II) and H-branch. $\Omega = 0.65$.

Figs. 18a-c: a) energy $E(t)$, b) solution $\Phi(x,t)$ and c) energy spectrum $\widehat{E}(\omega)$ of case with combined period doubling and quasiperiodicity. $\epsilon = 0.182$; $\Omega = 0.65$.

Figs. 19a-c: a) energy $E(t)$, b) solution $\Phi(x,t)$ and c) energy spectrum $\widehat{E}(\omega)$ of case with continuous spectrum but smooth space dependence. $\epsilon = 0.188$ in first continuum; $\Omega = 0.65$.

Figs. 20a-c: a) energy $E(t)$, b) solution $\Phi(x,t)$ and c) energy spectrum $\widehat{E}(\omega)$ of case with continuous spectrum but smooth space dependence. $\epsilon = 0.200$ in second continuum; $\Omega = 0.65$.

Figs. 21a-b: a) energy and b) solution in chaotic case. $\epsilon = 0.201$, $\Omega = 0.65$.

Fig. 22: State diagram $\epsilon(\Omega)$. Solid lines: catastrophic bifurcations; dotted lines: smooth bifurcations; dashed lines: drop from soliton chaos. Symbols $\bullet$, $\circ$, $+$, square, $\oplus$, and $\times$ denote constant, periodic, period-doubled, period-quadrupled or higher, quasiperiodic, and chaotic $E(t)$.

Fig. 23: State diagram $\epsilon(\Omega)$. Magnification of boxed area in Fig. 22.

Fig. 24: Spectrum $\widehat{\Phi}_k(\omega)$ for $k = 1$ of twisted-wave-type solution $\Phi(x,t)$ of Figs. 12a-c. $\omega > 0$ solid, $\omega < 0$ dashed.

Fig. 25: Spectrum $\widehat{\Phi}_k(\omega)$ for $k = 1$ of counterpropagating-wave-type solution $\Phi(x,t)$ of Figs. 4a-b.

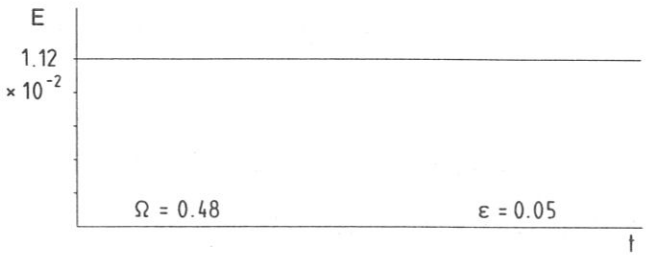

Figure 1a

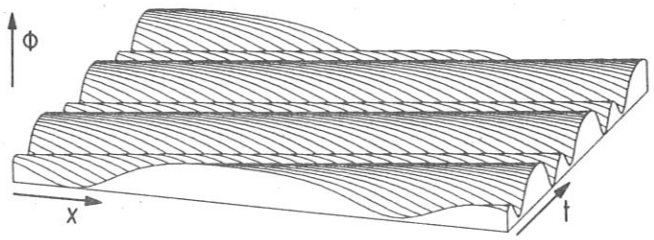

Figure 1b

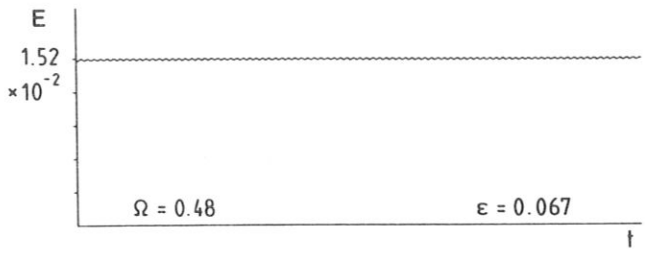

Figure 2a

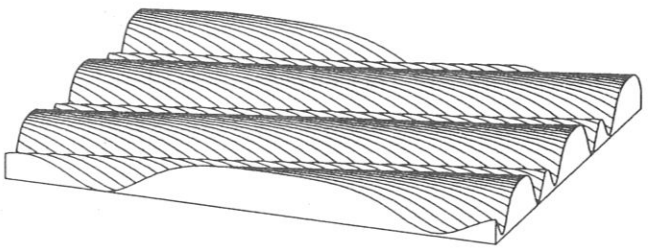

Figure 2b

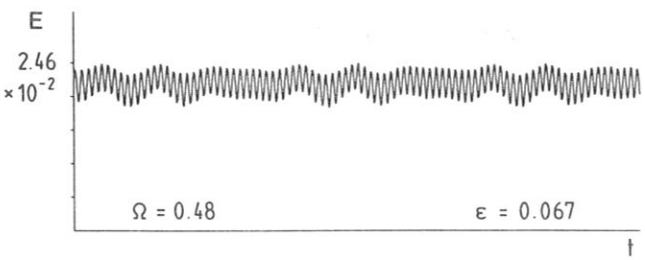

Figure 3a

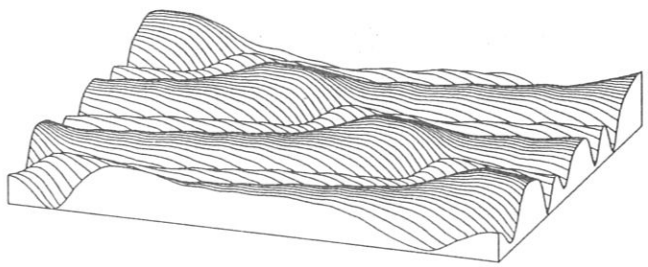

Figure 3b

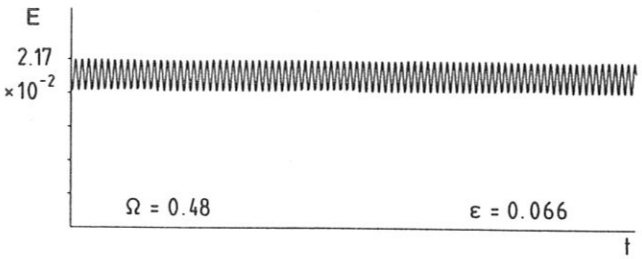

Figure 4a

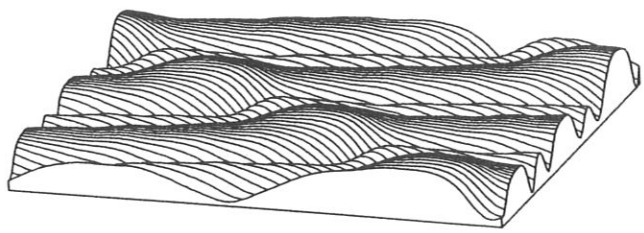

Figure 4b

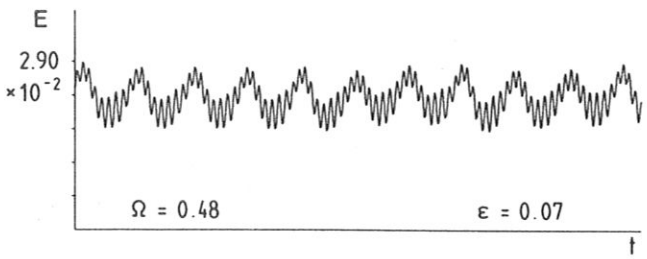

Figure 5a

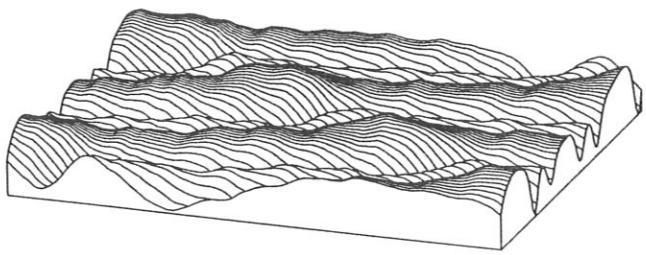

Figure 5b

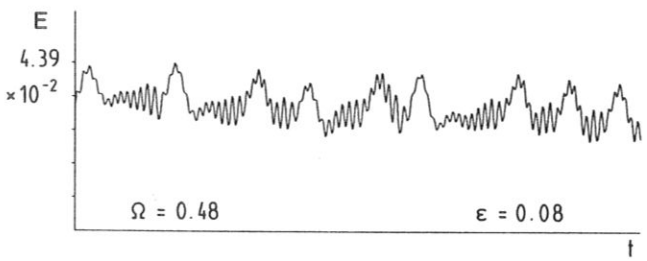

Figure 6a

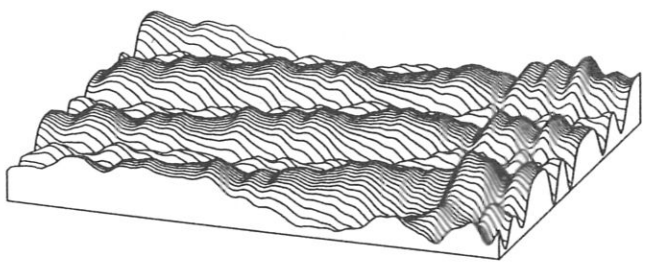

Figure 6b

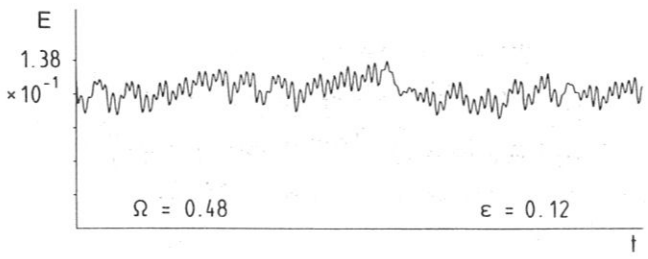

Figure 7a

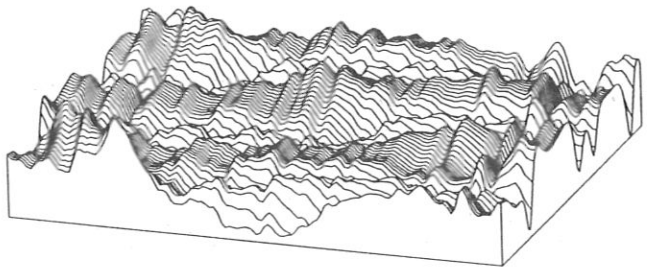

Figure 7b

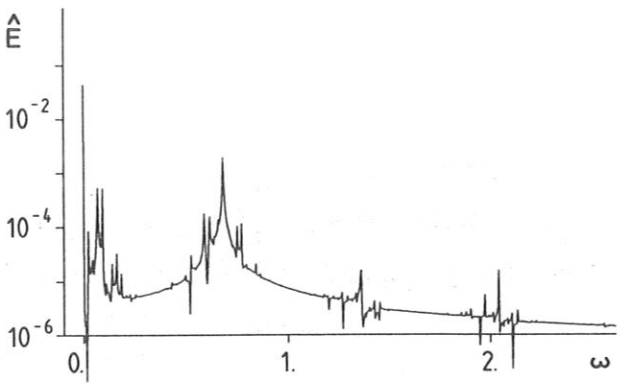

Figure 3c

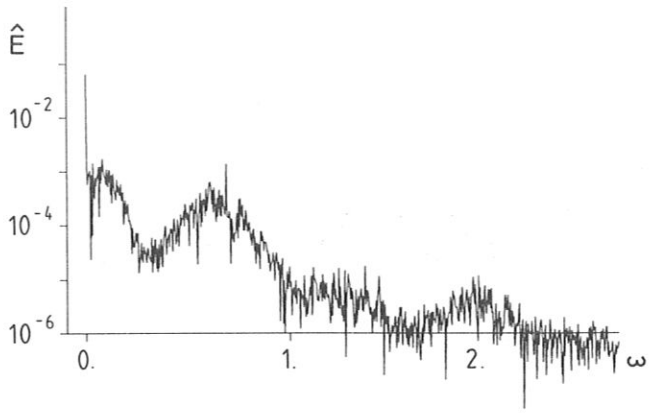

Figure 6c

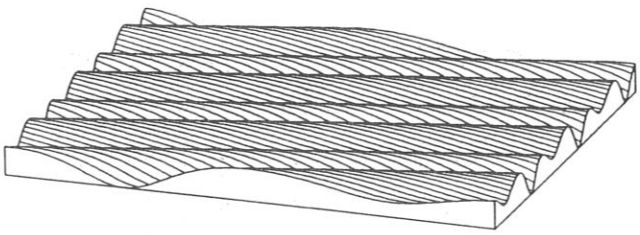

Figure 10a

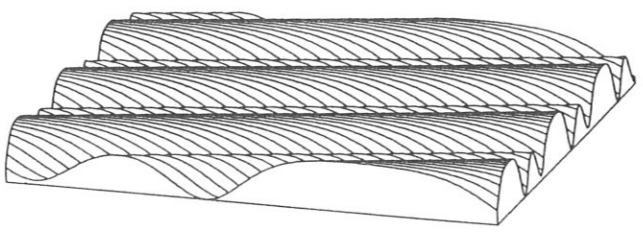

Figure 10b

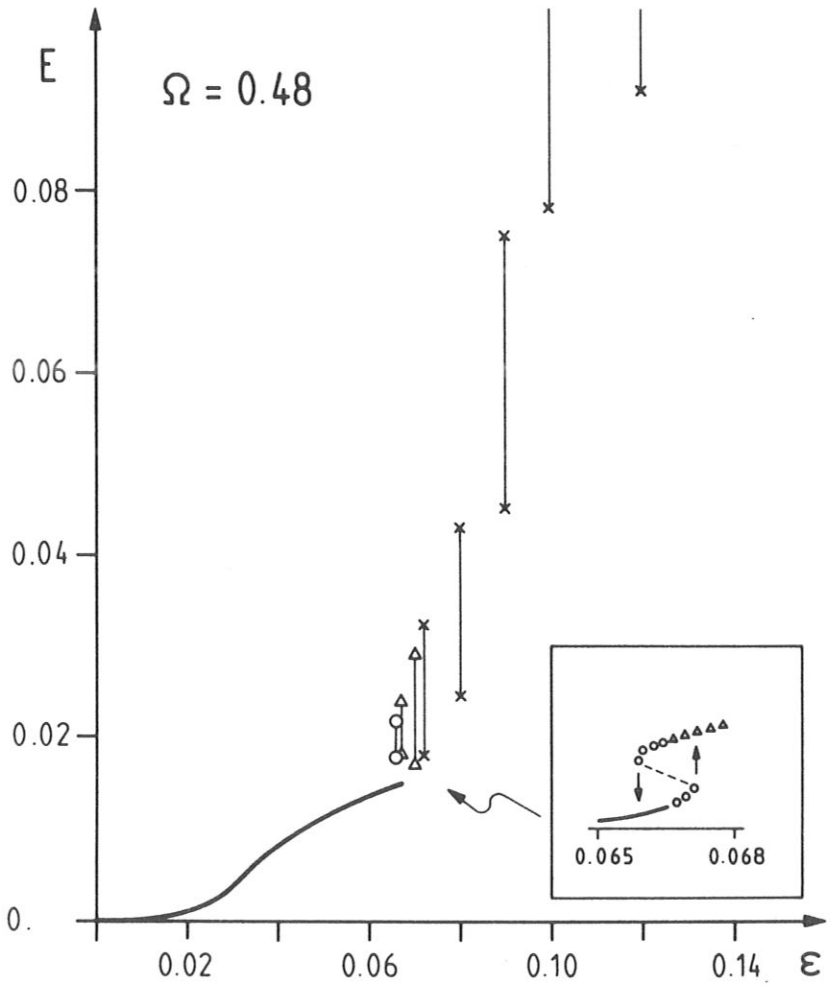

Figure 8

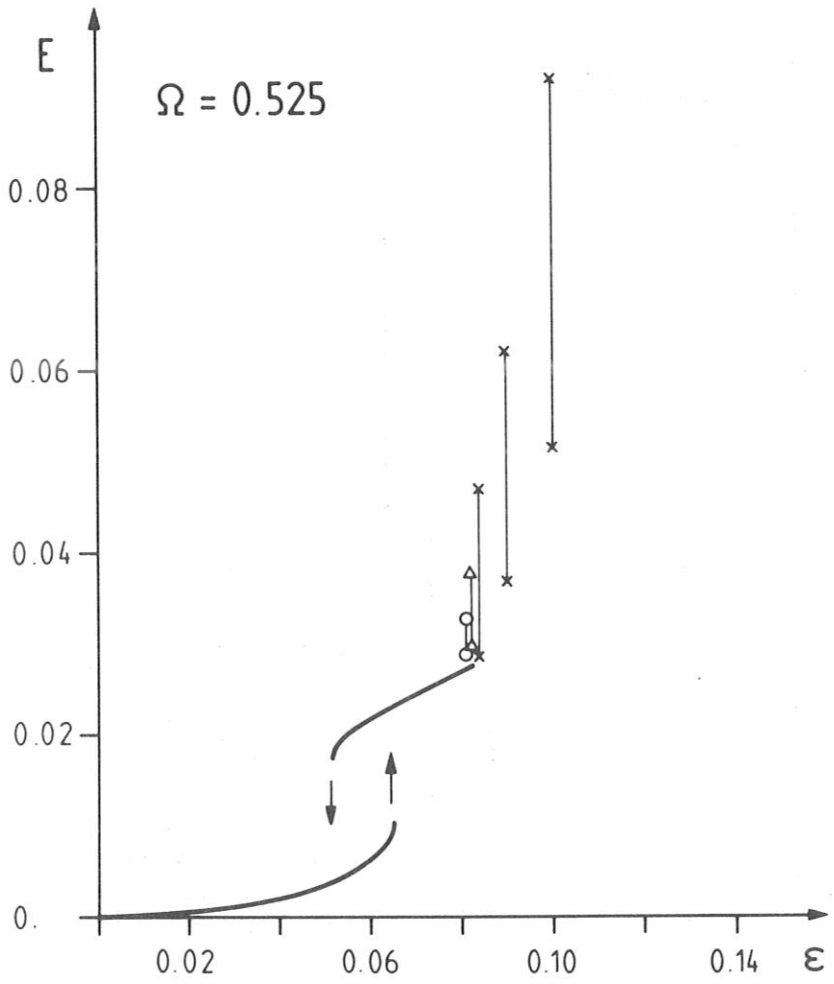

Figure 9

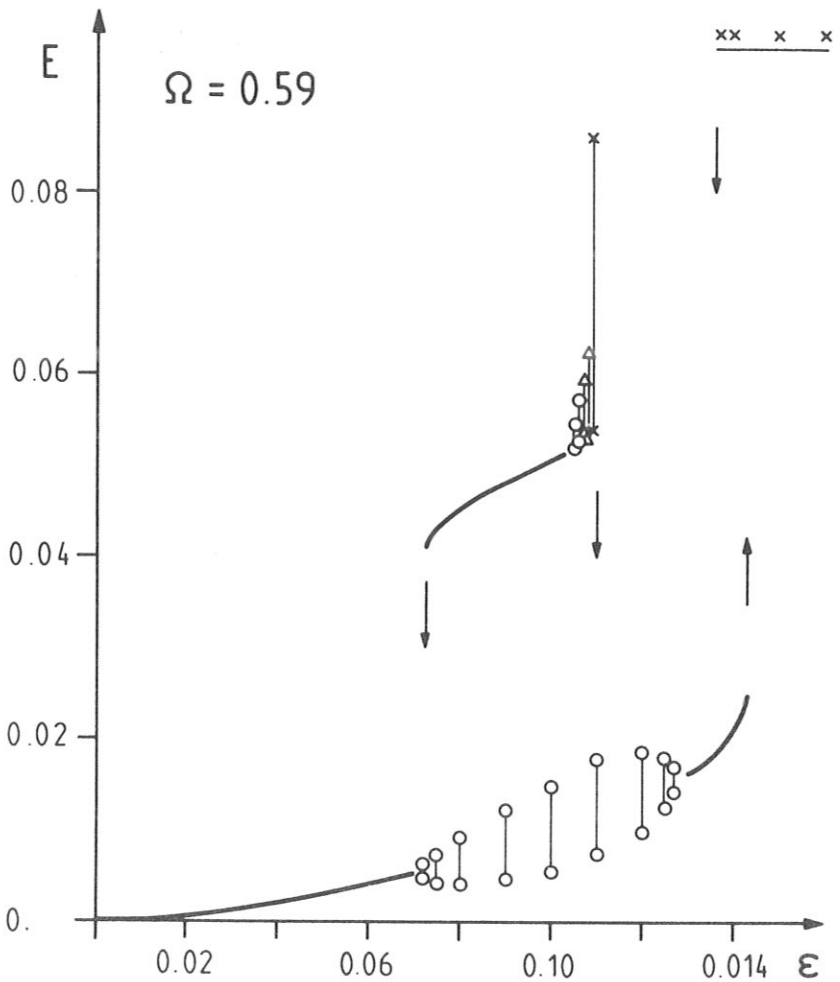

Figure 11

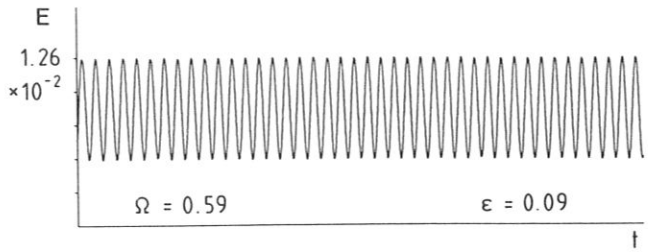

Figure 12a

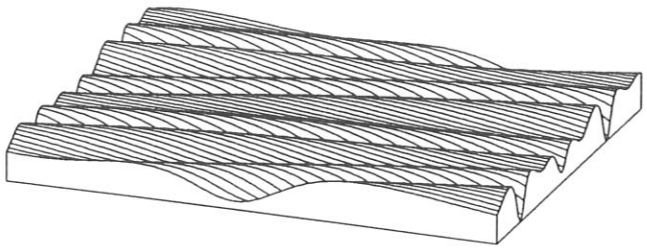

Figure 12b

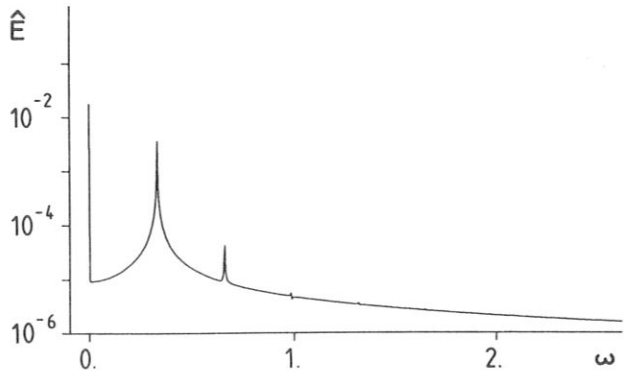

Figure 12c

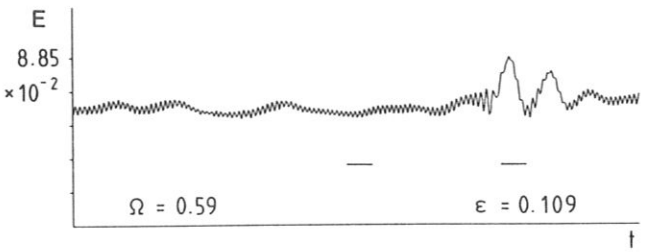

Figure 13a

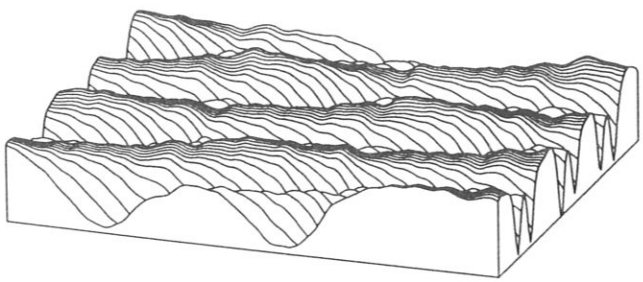

Figure 13b

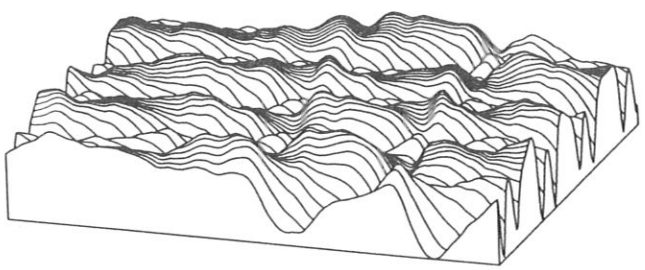

Figure 13c

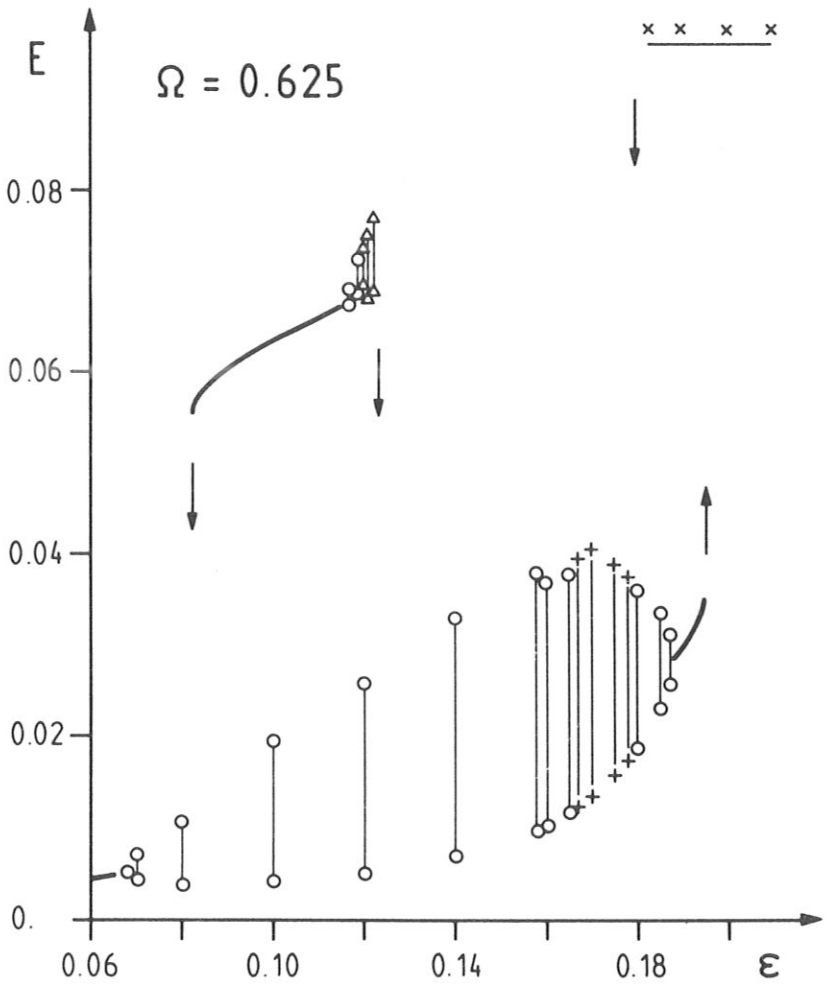

Figure 14

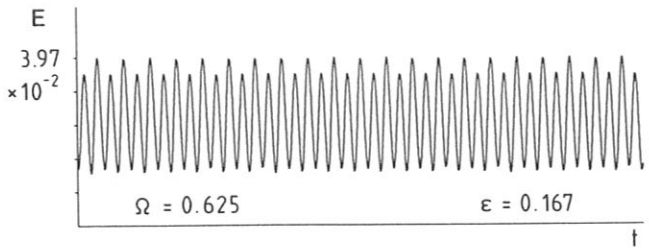

Figure 15a

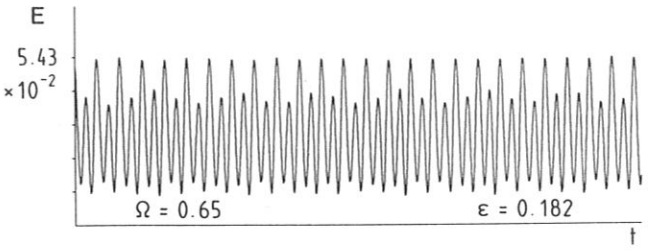

Figure 18a

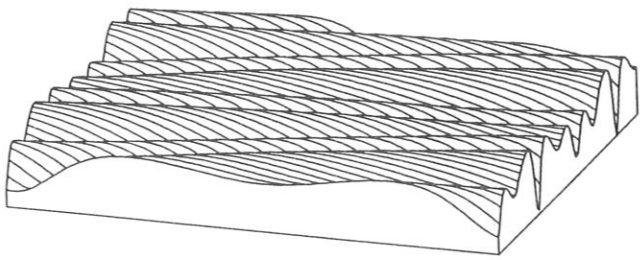

Figure 15b

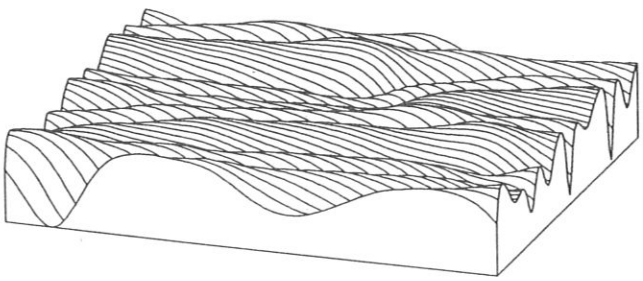

Figure 18b

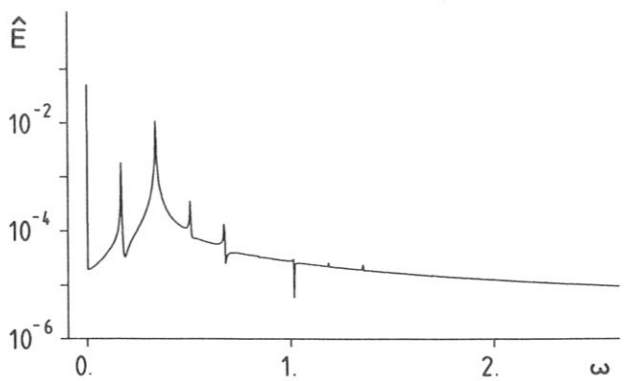

Figure 15c

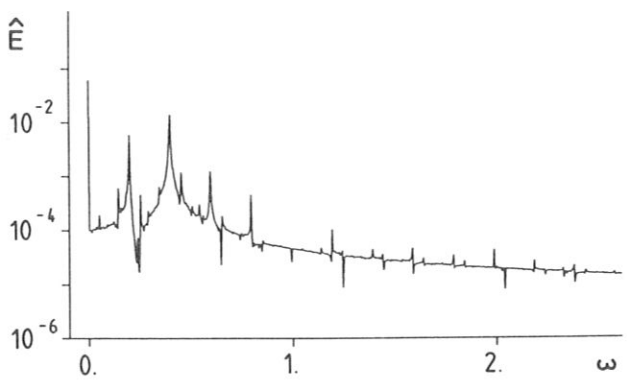

Figure 18c

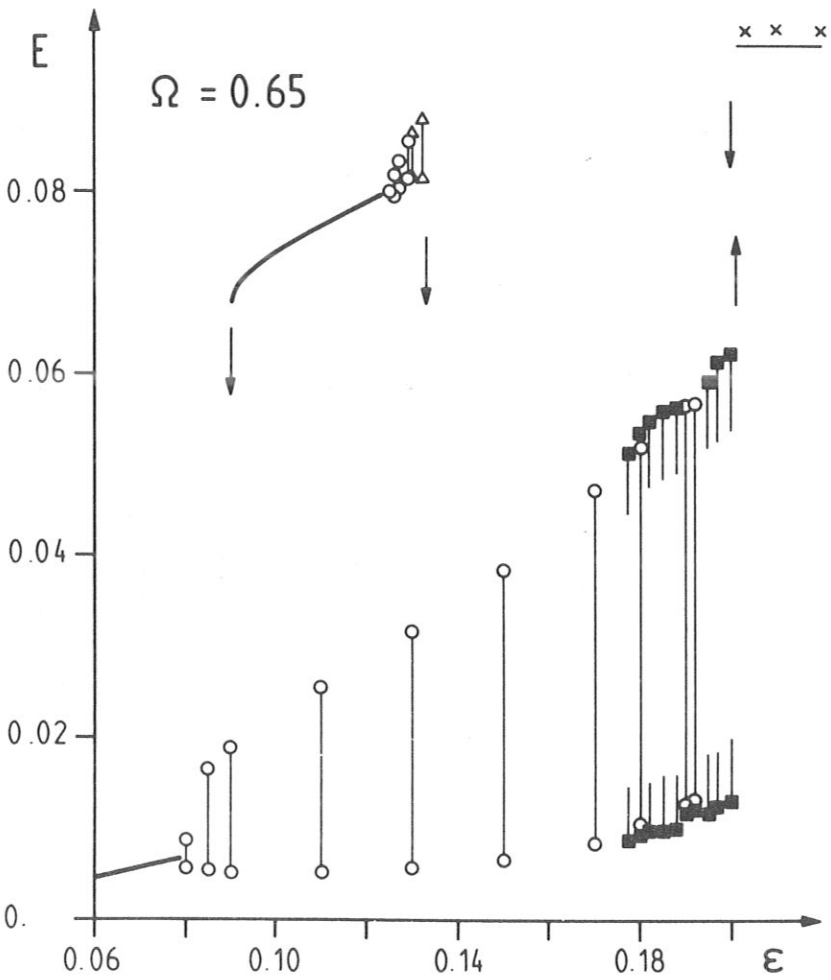

Figure 16

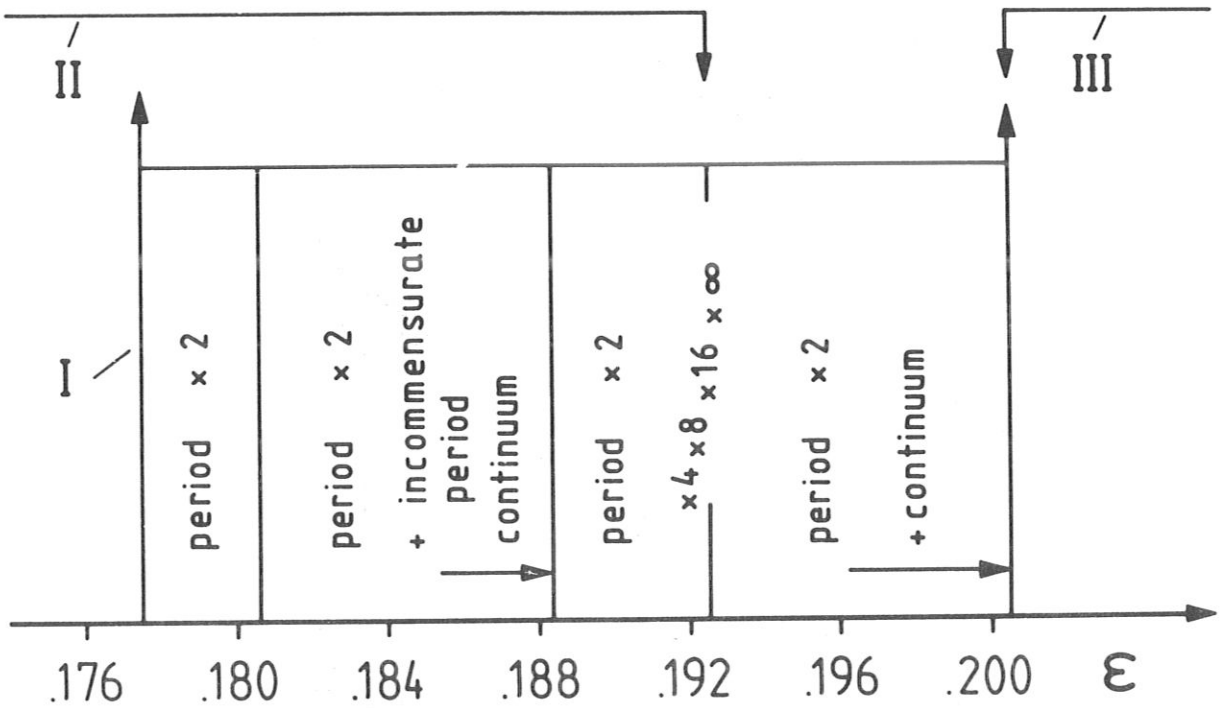
II
III
I
period × 2
period × 2
+ incommensurate period continuum
period × 2
× 4 × 8 × 16 × ∞
period × 2
+ continuum
.176
.180
.184
.188
.192
.196
.200
ε

Figure 17

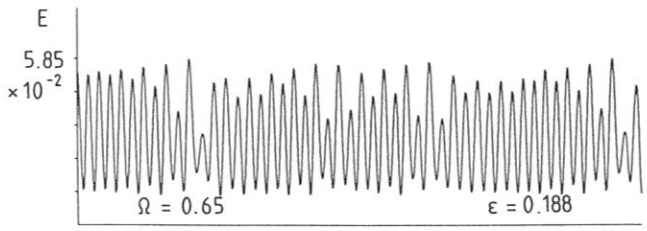

Figure 19a

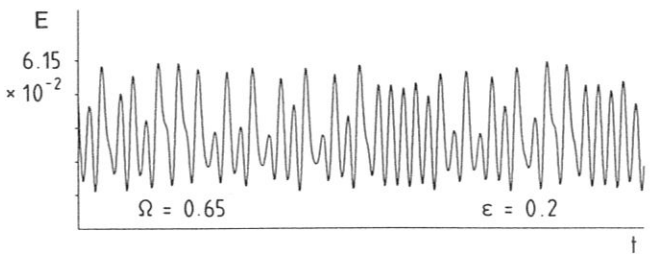

Figure 20a

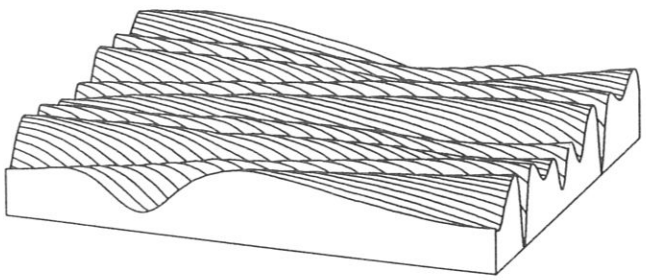

Figure 19b

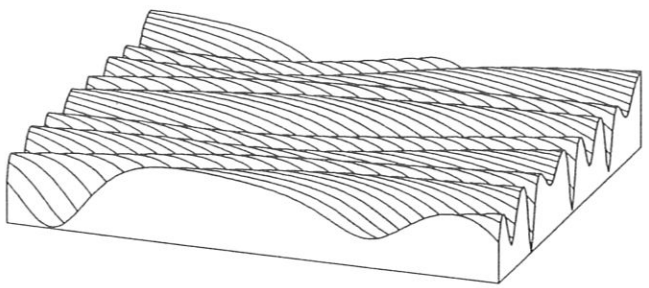

Figure 20b

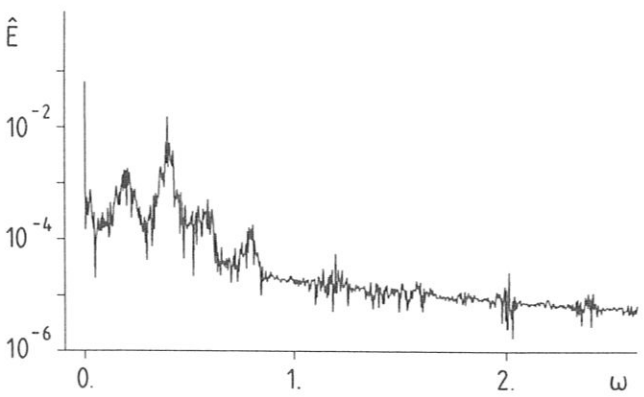

Figure 19c

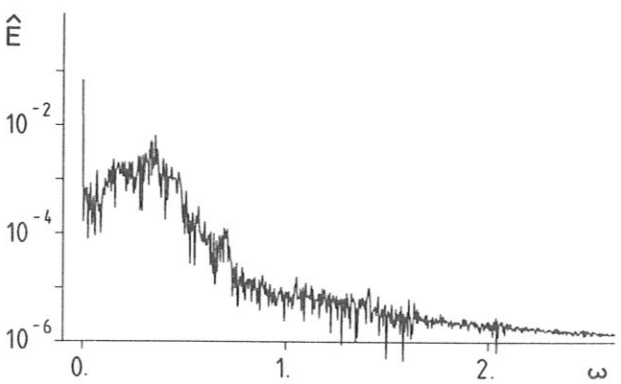

Figure 20c

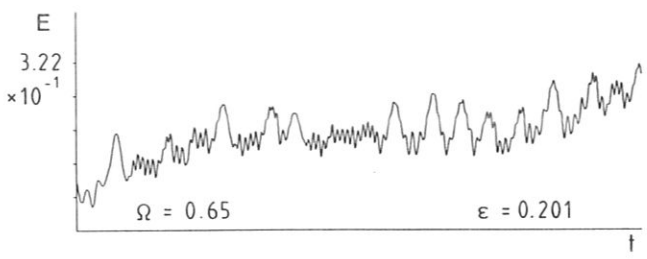

Figure 21a

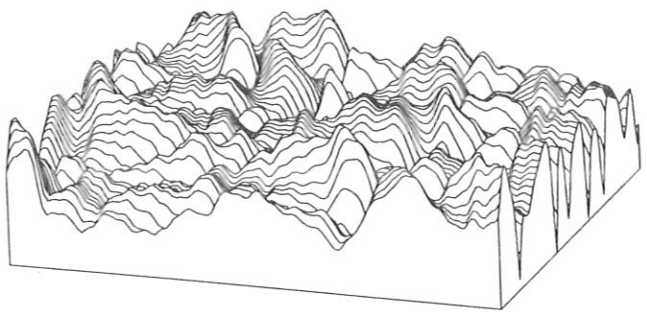

Figure 21b

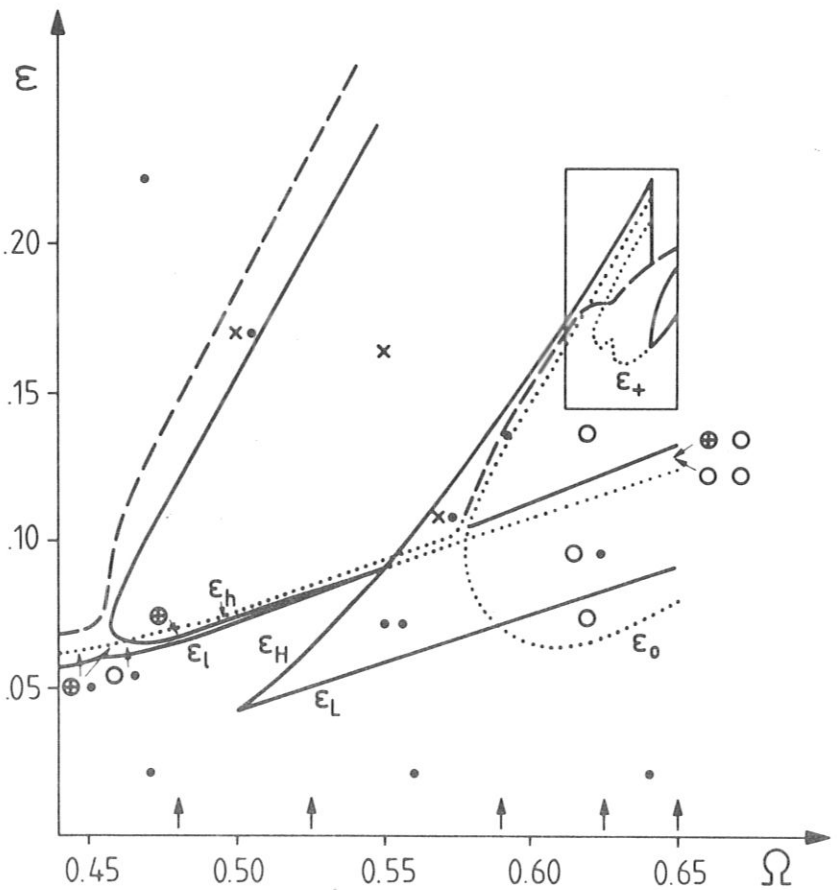

Figure 22

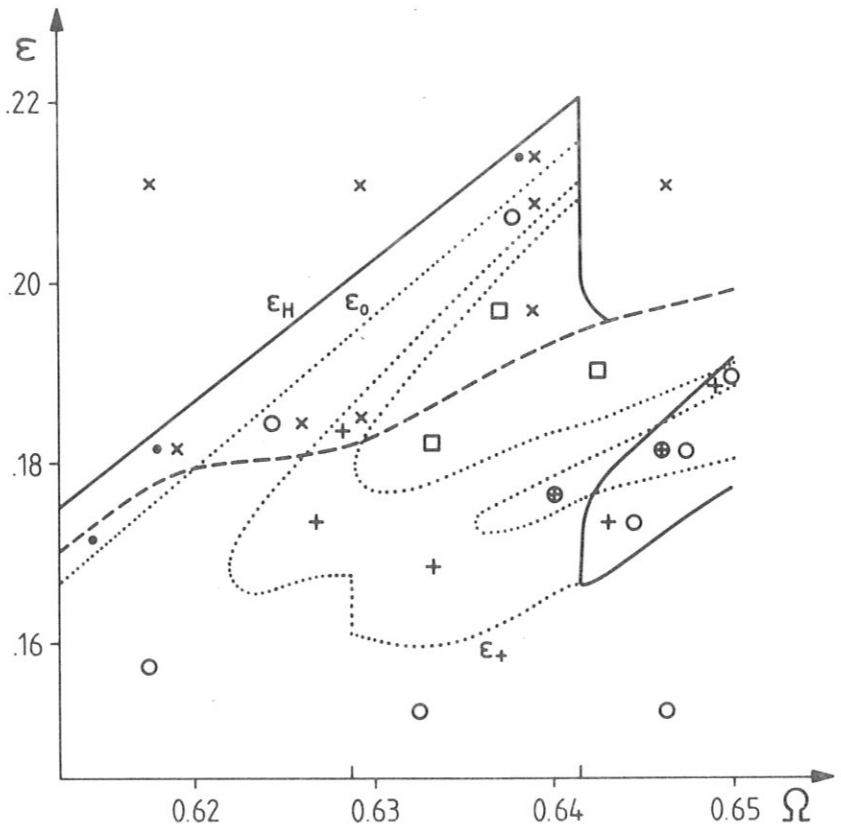
ε
.22
.20
.18
.16
ε_H
ε_0
ε_+
0.62
0.63
0.64
0.65
Ω

Figure 23

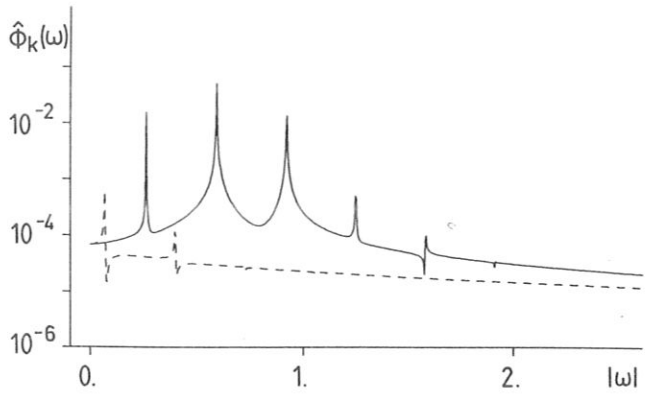

Figure 24

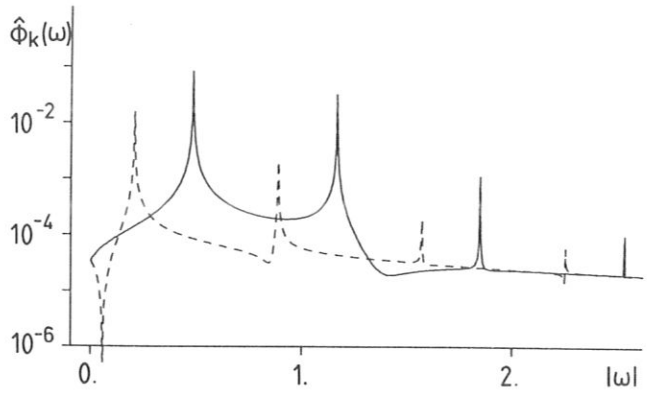

Figure 25